Available online at www.sciencedirect.com
ScienceDirect
International Journal of Heat and Mass Transfer 50 (2007) 1186–1195
International Journal of HEAT and MASS TRANSFER
www.elsevier.com/locate/ijhmt

Simulation of refrigerant flow boiling in serpentine tubes

H.L. Wu [a], X.F. Peng [a,*], P. Ye [a], Y. Eric Gong [b]

[a] Laboratory of Phase-change and Interfacial Transport Phenomena, Department of Thermal Engineering, Beijing 100084, China
[b] Advanced Heat Transfer LLC, 1715 Aaron Brenner Dr., Suite 726, Memphis, TN 38120, United States

Received 26 July 2005; received in revised form 8 August 2006
Available online 5 December 2006

Abstract

Numerical simulations were conducted to investigate the refrigerant flow boiling in a horizontal serpentine round tube with the Eulerian multiphase flow model and a phase-change model for the mass transfer. Correspondingly, an experimental investigation was conducted to provide validation and data for the simulations. The liquid/vapor phase distributions show stratification in horizontal tubes, indicating the buoyancy force caused by gravity acceleration is dominant, especially when the vapor void fraction is sufficiently high. The adiabatic bend sections served to redistribute the vapor phase, which was induced by the centrifugal force and re-condensation of the vapor (due to thermal non-equilibrium of two phases). The phase distributions in the bend sections showed the competitive influence of buoyancy force and centrifugal force at different operating conditions. In all cases, the numerical simulations appear reasonably consistent with the experimental observations. In particular, the simulation very well explains the bend effects on flow reconstruction and thermal non-equilibrium release observed in the experiments.
© 2006 Elsevier Ltd. All rights reserved.

Keywords: Serpentine round tube; U-bend; Simulation; Flow boiling; Phase distribution; Two-phase flow

1. Introduction

Serpentine tube evaporators are widely employed in modern energy conversion and power utility systems, HVACR engineering field and petrochemical industries. Though evaporators are very important in practical applications, the associated refrigerant flow boiling characteristics are still far from being fully understood because of its complexity in nature. Due to the shortage of appropriate guidance, present evaporators are usually designed with a profuse safety factor, resulting in unnecessary surface area and high superheat. Opportunities to take advantage of latent heat transfer by reducing refrigerant superheat can significantly reduce heat exchanger size and cost. Further understanding of flow boiling could lead to design of higher efficiency heat exchangers, thus further reducing manufacturing cost and energy consumption.

Convective flow boiling in tubes/channels has been investigated as a classical topic of boiling heat transfer in the open literature. Numerous investigations were conducted for horizontal, adiabatic gas–liquid two-phase flow in tubes [1–3]. Two-phase flow is a complicated physical process. In addition to inertia, viscous and pressure forces presented in single-phase flow, two-phase flows are also affected by interfacial tension forces, the wetting characteristics of the liquid on the tube wall and the exchange of momentum between the liquid and vapor phases in the flow. The traditional definition of the flow regimes of liquid–gas flow in a horizontal tube includes bubbly flow, plug flow, slug flow, wavy flow and annular flow [3]. Besides, there are other flow regimes also widely adopted, such as stratified flow, stratified/wavy flow, intermittent flow, mist flow, and so on. Theofanous and Hanratty [4] presented an overview of flow regimes in steady, fully developed multifluid flows. Depending on operating conditions and fluid properties, some of the aforementioned flow regimes may occur in evaporating two-phase flow systems.

* Corresponding author. Tel./fax: +86 10 6278 9751.
E-mail address: pxf-dte@mail.tsinghua.edu.cn (X.F. Peng).

0017-9310/$ - see front matter © 2006 Elsevier Ltd. All rights reserved.
doi:10.1016/j.ijheatmasstransfer.2006.10.013

Nomenclature

c_P	specific heat, J/(kg K)
d	diameter, m
G	mass flux, kg/(m^2 s)
g	gravitational acceleration, N/m
h	enthalpy, J/kg
h'	enthalpy of saturate liquid, J/kg
h''	enthalpy of saturate vapor, J/kg
h_{LH}	latent heat, $h_{LH} = h'' - h'$, J/kg
K_{jk}, K_{kj}	interphase momentum exchange coefficient
$\dot{m}$	mass flow rate, kg/s
T	temperature, K
Pr	Prandtl number
P_s	saturate pressure, Pa
Q	total heat input, W
q	heat flux, W/m^2
Re	relative Reynolds number
$\vec{R}_{jk}$	interphase force between phase j and k, N
t	time, s
τ_j	particulate relaxation time of the secondary phase, s
$S_{\dot{m}}$	interphase mass transfer source term, kg/(m^3 s)
u	velocity, m/s
X, Y, Z	coordinate in X, Y, Z-axis, respectively, m
x	thermal dynamical quality
α	volume fraction
λ	heat conductivity, W/(m K)
μ	viscosity, kg/(m s)
ρ	density, kg/m^3
σ	surface tension, N/m

Subscripts

in	inlet
out	outlet
l, v	liquid phase, vapor phase
j, k	jth phase, kth phase
p	particulate phase
s	saturate

Flow pattern maps were developed to predict the flow regimes and the vapor–liquid flow configurations in two-phase flows. The flow pattern map proposed by Taitel and Dukler [2] was widely applied for adiabatic two-phase flow, which identified the flow regime as a function of Martinelli parameter X_{tt}. Later, Hashizume et al. [5] found that the boundaries or transitions of flow pattern, in the flow pattern map for boiling refrigerant two-phase flows, differs significantly from those presented in adiabatic two-phase flows. Actually, for flow boiling processes, mass transfer plays an important role in the dynamic phase distribution and hence flow regime. The adiabatic flow pattern maps, such as Baker map or Taitel and Dukler map, showed poor accuracy of prediction of flow regime in adiabatic two-phase flows. Based on Taitel and Dukler map, Steiner [6] developed an adiabatic flow pattern map based on R-12 and R-22 data. Recently, Kattan et al. [7–9] improved Steiner map by modifying the axes of the map for handier application to evaporating flows and by including the influences of heat flux and dryout on the flow regime transition. The new flow pattern map was based on R-134a, R-123, R-402A and R-404A data under evaporating conditions and could be applied to both adiabatic and non-adiabatic two-phase flows. They also developed a new flow-boiling model based on local flow patterns. Thome and Hajal [10] presented a simpler method to get the equivalent results of Kattan map. The newest version of Kattan map was proposed by Wojtan [11], which considered dynamic void fraction and cross-sectional locus of the liquid–vapor interface, and the effects of heat flux on the transition to mist flow. Kandlikar [12] presented a modified correlation for flow boiling in circular tubes with experimental data covering working fluids of water and several refrigerants. Thome et al. [13,14] proposed a new flow pattern map and void fraction equation for condensation in horizontal tubes, which was used to develop a new flow pattern based condensation heat transfer model for condensation. So far, most of the available research have been conducted for straight tubes, and particularly very limited investigations have been done to understand the flow boiling in serpentine tubes.

In present paper, numerical simulations were conducted to investigate the flow boiling characteristics in horizontal serpentine tubes using refrigerant R-141B as the working fluid. The simulation results are analyzed and compared with experimental observations.

2. CFD simulation

2.1. Multiphase flow models

The flow boiling process was simulated using the CFD software Fluent 6.2 with user-developed subroutines. Eulerian multiphase flow model was applied for the two-phase flow, where both phases were treated as interpenetrating continually with the flow behavior described by Navier–Stokes equations. The liquid and vapor were set as the primary and secondary phase, respectively. This model is appropriate for the flow boiling modeling because it handles the full coupling between the phases and provides interphase drag laws and separate phase turbulence modeling.

The conservation equations for each phase are similar to those of single-phase flow, but modified by introduction of phasic volume fractions and derived to obtain a group of

equations with similar structures. In liquid–vapor two-phase flow the void fraction is defined by the phasic volume fraction, or the space occupied by the gas phase. Void fraction is one of the most important parameters which determines the flow patterns and the velocities of each phase. In order to account for the effects of turbulence transfer between phases, the turbulence model for each phase is applied [14]. The Realizable k–ε turbulence model [15] was applied together with two-layer enhanced wall function treatment for the near wall turbulence modeling.

Conservation equations solved included modified equations for mass (Eq. (1)), momentum (Eq. (2)), energy, turbulence kinetic energy and its dissipation rate [16].

$$\frac{\partial}{\partial t}(\alpha_k\rho_k)+\nabla\cdot(\alpha_k\rho_k\vec{u}_k)=\sum_{j=1}^{n}S_{\dot{m},jk} \tag{1}$$

$$\frac{\partial}{\partial t}(\alpha_k\rho_k\vec{u}_k)+\nabla\cdot(\alpha_k\rho_k\vec{u}_k\vec{u}_k)=-\alpha_k\nabla p+\nabla\cdot\bar{\bar{\tau}}_k+\sum_{j=1}^{n}(\vec{R}_{jk}+\dot{m}_{jk}\vec{u}_{jk})+(\vec{F}_k+\vec{F}_{lift,k}+\vec{F}_{vm,k}) \tag{2}$$

The volume fraction of each phase was calculated from a continuity equation:

$$\frac{\partial}{\partial t}(\alpha_k)+\nabla\cdot(\alpha_k\vec{u}_k)=\frac{1}{\rho_k}\left(\sum_{j=1}^{n}\dot{m}_{jk}-\alpha_k\frac{d_k\rho_k}{\mathrm{d}t}\right) \tag{3}$$

along with

$$\sum_{k=1}^{n}\alpha_k=1 \tag{4}$$

The coupling of equations is realized by constitutive relations between two phases. Among those constitutive relations, the most important one is the interphase force between phase j and k, $\vec{R}_{jk}$, which depends on the friction, pressure, cohesion. It is calculated using a simple interaction term.

$$\sum_{j=1}^{n}\vec{R}_{jk}=\sum_{j=1}^{n}K_{jk}(\vec{u}_j-\vec{u}_k) \tag{5}$$

where $K_{jk}=K_{kj}$ is the interphase momentum exchange coefficient,

$$K_{jk}=K_{kj}=\frac{\alpha_k\alpha_j\rho_j f}{\tau_j} \tag{6}$$

where f is the drag function based on the relative Reynolds number Re, $f=\frac{C_D Re}{24}$ (C_D is calculated using Schiller and Naumann's model [17]), and τ_j the particulate relaxation time of the secondary phase, $\tau_j=\frac{\rho_j d_j^2}{18\mu_k}$.

The phase-change mass and heat transfer are modeled by user-defined source terms in the continuity and energy equations. To calculate the heat transfer coefficient between the jth and kth phase, Ranz and Marshall's Model [18,19] was applied. It assumes the heat transfer coefficient at the vapor side of the dispersed phase is infinite, and the liquid side (particulate phase) Nusselt number could be described as follows:

$$Nu_{\mathrm{p}}=2.0+0.6Re_{\mathrm{p}}^{1/3}Pr^{1/3} \tag{7}$$

The interphase mass transfer source term $S_{\dot{m},jk}$ in Eq. (1) is related with phase change. The model of Lee [20] is applied, which defines the mass transfer during the process of evaporating or condensing. The phase change is assumed to be at a constant pressure and at a quasi thermo-equilibrium state. The mass transfer from liquid to vapor and that from vapor to liquid are given by the following equations:

$$S_{\dot{m},\mathrm{lv}}=\begin{cases}r_{\mathrm{lv}}\alpha_{\mathrm{l}}\rho_{\mathrm{l}}(T_{\mathrm{l}}-T_{\mathrm{s}})/T_{\mathrm{s}} & T_{\mathrm{l}}\geqslant T_{\mathrm{s}}\\ 0 & T_{\mathrm{l}}<T_{\mathrm{s}}\end{cases} \tag{8a}$$

$$S_{\dot{m},\mathrm{vl}}=\begin{cases}r_{\mathrm{vl}}\alpha_{\mathrm{v}}\rho_{\mathrm{v}}(T_{\mathrm{s}}-T_{\mathrm{v}})/T_{\mathrm{s}} & T_{\mathrm{v}}\leqslant T_{\mathrm{s}}\\ 0 & T_{\mathrm{v}}>T_{\mathrm{s}}\end{cases} \tag{8b}$$

where r_{lv} and r_{vl} are mass transfer time parameters with unit s^{-1}. In the problem here, r_{lv} and r_{vl} are set to be 0.1.

The Phase Coupled SIMPLE algorithm (Vasquez and Ivanov [21]) was used for the pressure–velocity coupling. The block algebraic multigrid scheme used by the coupled solver is used to solve a vector equation formed by the velocity components of all phases simultaneously. A pressure correction equation is then built, based on total volume continuity rather than mass continuity. Pressure and velocities are corrected so as to satisfy the continuity constraint.

Compared to other multiphase flow models, the Eulerian model is more general and sophisticated, but it also requires more memory allocation and is less robust with weaker convergence and stability. A transient simulation was chosen to obtain a convergent solution. The evolution of flow boiling was tracked by transient simulation until a quasi-steady solution was reached. The time step for such multiphase flow simulation was typically 1×10^{-5} s.

2.2. Geometry and boundary conditions

The flow boiling process in a horizontal serpentine tube was investigated using refrigerant R-141B as the working fluid. Fig. 1 shows the simulated serpentine tube and the corresponding test module in the visualization experiment. The serpentine test tube consisted of four straight sections and three U-bends. The straight sections marked with length 80 mm in Fig. 1a were heated with uniform heat flux. "R26" and "R34" indicate that the outer and inner radius of the bend are 26 and 34 mm, respectively. The coordinate is set as shown in Fig. 1a, with the gravitation acceleration ($g=9.8\ \mathrm{m/s^2}$) in the negative Z-axis.

The system pressure, P_{s}, is 101,325 Pa. The saturation temperature of R-141B, T_{s}, is 308.15 K and the latent heat h_{LH} is 222.8 kJ/kg. At the inlet, a single-phase liquid flow is set with a constant velocity and a subcooling of 3 K. Three cases are simulated with different mass fluxes and heat input, as listed in Table 1, where Q is the total heat input through the wall of the four straight heated sections, q the heat flux at the heated sections, u_{in} the liquid velocity entering the serpentine test tube, and G the mass flux,

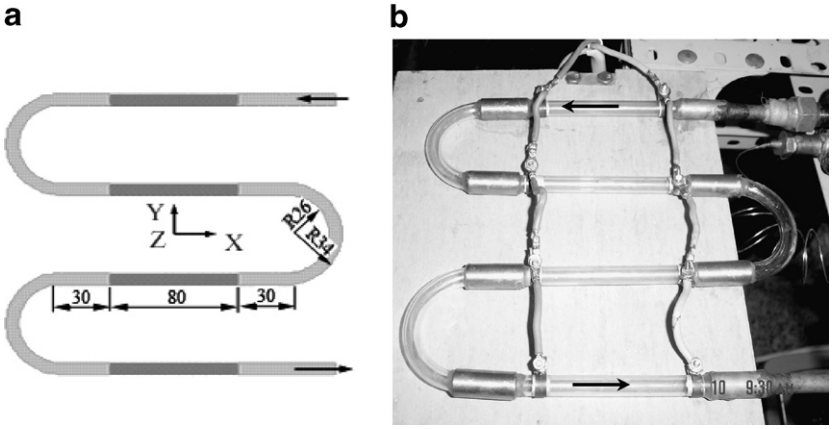

Fig. 1. Serpentine tube and geometry: (a) simulation model (unit: mm); (b) test section.

Table 1
Operating parameters in simulations

	q (W/m^2)	Q (W)	u_{in} (m/s)	G (kg/(m^2 s))	x
Case 1	7211	58	0.033	40	0.11
Case 2	7211	58	0.17	200	0.01
Case 3	36055	290	0.17	200	0.11

$G = \rho_l \cdot u_{in}$. The outlet thermal dynamical quality x is calculated by,

$$x = \frac{Q - Q_l}{\dot{m} h_{LH}} = \frac{Q - c_{p,l}\dot{m}(T_{in} - T_s)}{\dot{m}(h'' - h')} \tag{9}$$

where Q_l is the heat absorbed by the liquid to reach the saturation liquid state, $\dot{m}$ the mass flow rate, and h' and h'' the enthalpy of the saturation liquid and saturation vapor, respectively.

Before the multiphase flow model was activated, the steady-state isothermal liquid flow was obtained by solving the governing equations except for the energy equation. Then the simulated flow field was used as an initial condition for the multiphase flow modeling. This treatment, establishing the isothermal flow first, was also accordant to the practical flow boiling process in the experiment.

For the transient flow boiling process simulated with the Eulerian model, each case took about 10 days to solve on a personal computer with dual 3.2 GHz processor and 4 G RAM and windows XP operating system.

3. Experiment

To explore the fundamental phenomena and characteristics of refrigerant flow boiling and to provide important experimental evidences to validate the simulation, an experimental investigation was also conducted. The test facility is shown in Fig. 2. The working fluid was circulated in a closed loop, consisting in series of a liquid tank, a pump, a flow meter, a pre-heater, a pre-mixing chamber, the test section, a post-mixing chamber, a filter and a condenser. The pre- and post-mixing chambers were designed to provide a uniform flow condition through the test section. The flow pattern in the transparent quartz tube test

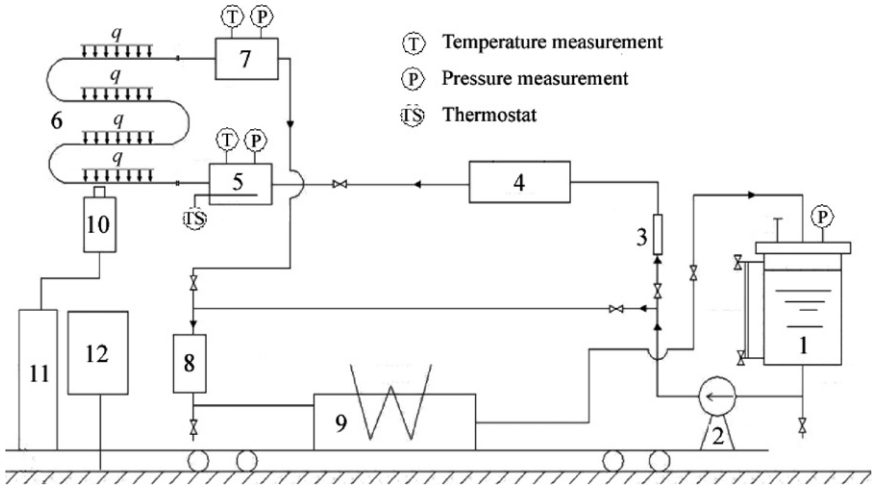

Fig. 2. Sketch map of test facility: (1) tank; (2) pump; (3) flow meter; (4) pre-heater; (5) pre-mixing chamber; (6) test section; (7) post-mixing chamber; (8) filter; (9) condenser; (10) CCD; (11) computer; (12) circuit controller.

section was recorded by a high-speed CCD video system (at a speed of 50 frame/s up to 15,000 frame/s dependent upon the experimental conditions) and transferred to a computer for further analysis.

The test section was a serpentine tube ($\varnothing$ 10 × 1 mm) made of smooth quartz glass, which had high temperature durability, low thermal expansion and high transparency. The dimensions are shown in Fig. 1a. In the straight sections, the outer surfaces were coated with optically transparent electric-conducting metal oxide film. Copper connectors joined the straight sections and the bends and functioned as the electrodes for electrically heating of the metal oxide film. A voltage regulator adjusted the heating power. The tube U-bend sections were not directly heated and hence treated as adiabatic. The experiments were conducted at different heat fluxes and mass fluxes in the serpentine tube.

4. Flow boiling behavior

4.1. Flow patterns

Taking Case 2 as an example, the simulated contours of near-wall vapor void fraction are shown in Fig. 3, and the corresponding cross-sectional area-averaged vapor void fractions at different locations are presented in Table 2. The vapor generation occurs in all heated straight sections, and the adiabatic bends serve to redistribute the vapor due to the geometric changes and possible vapor re-condensation, which may be induced by the thermal non-equilibrium between the two phases. The side view of the phase distributions shows that stratified or wavy flow is the primary flow regime in the boiling process in the horizontal serpentine tube. It also shows that boiling nucleation occurs at the top of the tube.

For the operating condition with mass flux ranging from 40 to 200 kg/(m^2 s), bubbly flow, churn flow, slug flow, stratified/wavy flow were experimentally observed in the serpentine tube. Fig. 4 presents the images of different flow patterns developed in the straight sections along the serpentine tube. The illustration map of flow regime evolution during the flow boiling in a horizontal straight tube is also depicted in Fig. 4. The part in a dashed line frame presents the flow regime evolution at higher vapor qualities according to Collier and Thome's flow regime map [3].

Table 2
Cross-sectional area-averaged void fractions for Case 2

First bend exit	Second bend exit	Third bend exit	Outlet
0.015	0.022	0.055	0.156

In order to quantitatively validate the modeling method, the local void fraction obtained from the simulation and the experiment data were compared. In the visualization experiment, the interface between the liquid and vapor phases at different locations (mainly at the bends) was distinguished from a series of video frames, and the time-averaged value was used to calculate the volume fractions. In the numerical simulation, the quasi-steady solution was used to gain the corresponding results. For Case 1, the calculated void fraction at the outlet is 0.73, and the measured value is about 0.83. The comparison between the numerical result and experimental data shows reasonable agreement. It is also close to the result calculated by Rouhani and Axelsson's correlation for horizontal tubes [22] (Eq. (10)), which is 0.78 for Case 1.

$$\alpha_v = \frac{x}{\rho_v}\left[(1+0.12(1-x))\left(\frac{x}{\rho_v}+\frac{1-x}{\rho_l}\right)+\frac{1.18(1-x)[g\sigma_l(\rho_l-\rho_v)]^{0.25}}{G\rho_l^{0.5}}\right]^{-1} \tag{10}$$

where σ_l is the surface tension of the liquid.

Although the general feature of phasic distributions can be captured by the numerical simulation, the dynamic or intermittent characteristic cannot be predicted. Therefore the slug flow and intermittent stratified/wavy flow can hardly be illustrated as observed in experiments. Besides, there are some other effects of nucleation, which are observed in the experiments but not included in the simulation, such as nucleation promoted by dissolved gases or other foreign matters. Nevertheless, the predicted phase distributions are in good agreement with the experimental observations. This implies that the buoyancy force is determinant in the nature of flow boiling in horizontal tubes evaluated in this study.

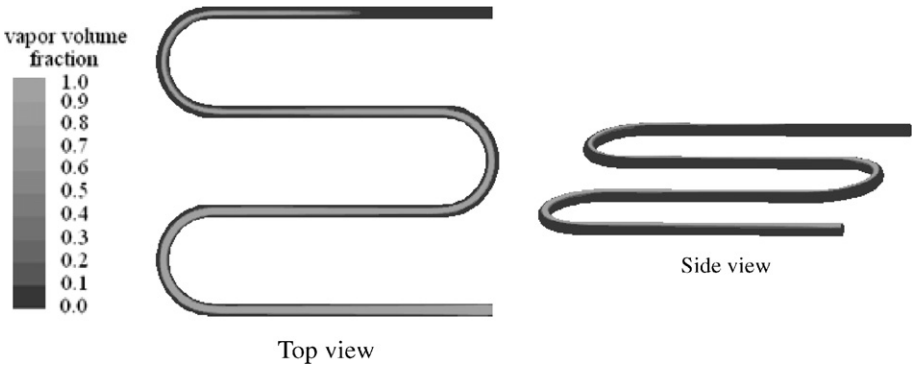

Fig. 3. Contours of near-wall vapor void fraction for Case 2.

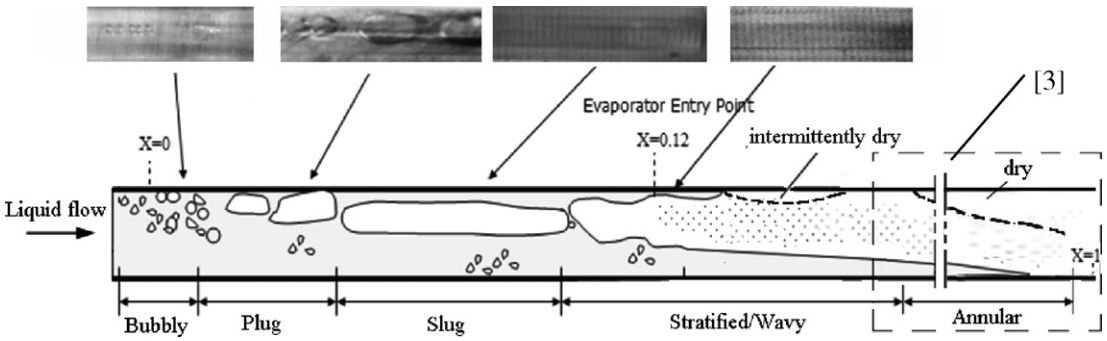

Fig. 4. Typical flow regimes observed in a horizontal serpentine tube evaporator.

4.2. Flow in the U-bends

The U-bend region is an important feature of the serpentine tube evaporator. Though the bends are not heated in the present experiments or some practical applications, they have significant influences on the phase distributions at the U-bends and their immediate downstream regions. Fig. 5 illustrates the phase distributions at the cross sections of the bends obtained from the present simulation and the side view photos in the experiment for Case 1. Both simulation and experimental observation show the typical stratification of the two-phase flow. For an actual flow boiling system, instabilities always exist due to the dynamic behavior of phase transition and two-phase interfacial instability. This causes the break up of the continuous vapor space, as shown in Fig. 5f. Fig. 6 displays the top view phase distributions at the third bend for Case 3. Both simulation and experimental results indicate that vapor is closer to inner wall of the bend section.

Besides the vapor–liquid stratification, the interface between the vapor and liquid is slightly tilted from the Z-axis. The vapor preferably accumulates in the upper-inner part of the bends, which could also be observed in Figs. 5 and 6. With higher mass flux, this phenomenon becomes more evident (see Fig. 7). The analysis for these cases shows slightly higher vapor velocity than liquid velocity, so we attribute buoyant force and centrifugal forces as influence factors for the phase redistributions at the U-bends.

4.3. Boiling evolution

Fig. 8 shows the evolution of near-wall vapor void fraction during the transient flow boiling process for Case 3. In Fig. 8a, the boiling starts at the upper parts of the heated sections, with vapor entrained downstream by the bulk flow. In Fig. 8b, when the vapor arrives at the U-bends, the two-phase flow is influenced with phase redistribution starting to appear. Later, in Fig. 8c, the phase distributions

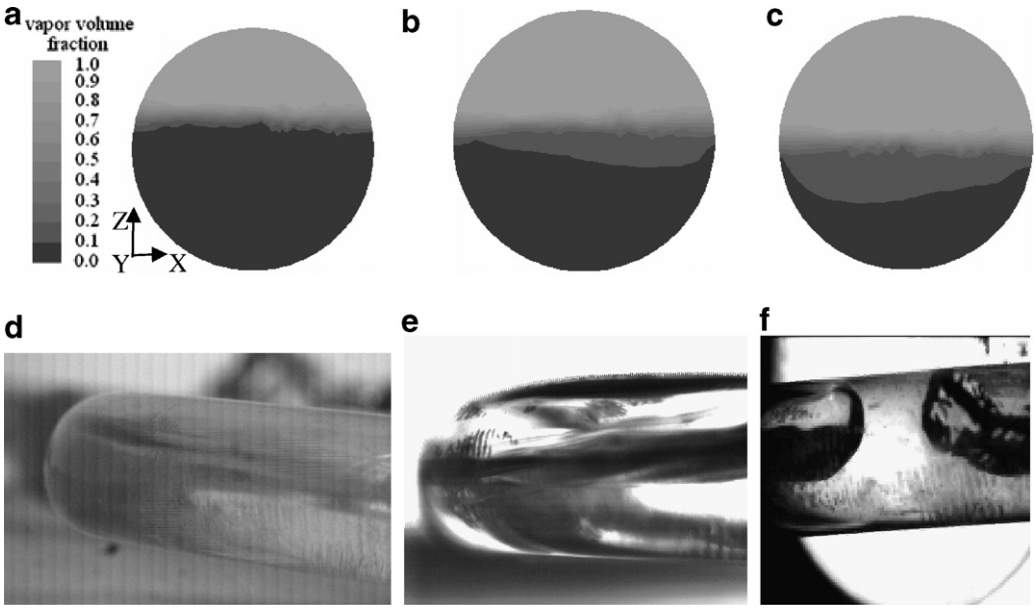

Fig. 5. Phase distributions at bends for Case 1 (side view): (a) first bend, (b) second bend, (c) third bend, (d) photo at first bend, (e) photo at second bend and (f) photo at third bend.

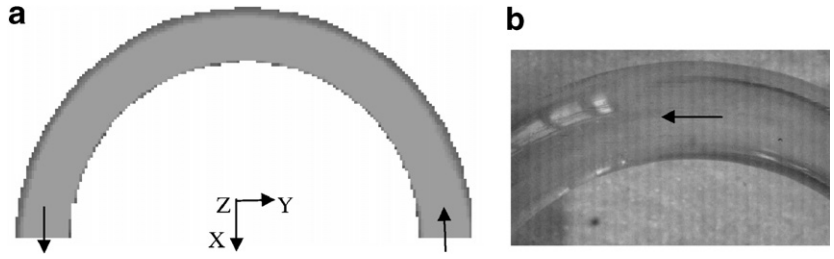

Fig. 6. Phase distributions at the third bend for Case 3 (top view): (a) simulation (contour legend same as that in Fig. 5) and (b) photo.

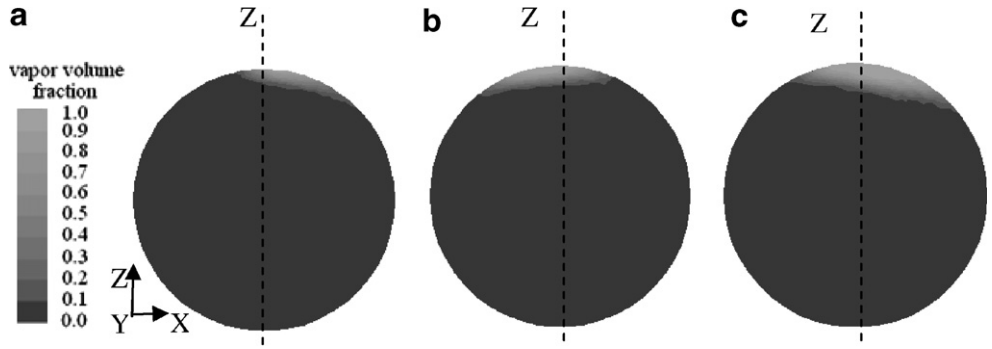

Fig. 7. Phase distributions at the bends for Case 2 (cross-sectional view): (a) first bend, (b) second bend and (c) third bend.

at the heated section begin to be influenced by the upstream sections. In Fig. 8d, the steady-state two-phase flow pattern is almost established. However, the phase redistributions at the bends are still developing. The flow boiling process reaches the steady-state after 24 s, as shown in Fig. 8e.

The flow and phase distribution in bend regions are further investigated taking the third bend as an example. Before the mixture reaches the bend, the flow normally presents a very well stratified regime due to buoyancy. Once it enters the bend, the liquid–vapor interface begins to tilt, with the liquid going straight and occupying the outside of the bend and the vapor squeezing to the inner side of the bend forming a "twisted" flow pattern. Then, during the flow in the bend, the vapor remains in the inward part while the liquid outward. This indicates that the centrifugal force plays an increasing role in the bends. As the mixture flows out of the bend, the centrifugal force is decreased due to the gradually smaller flow curvature, and the buoyant force recovers to become dominant, resulting in a stratification regime once more. To some extent, a quasi-symmetric

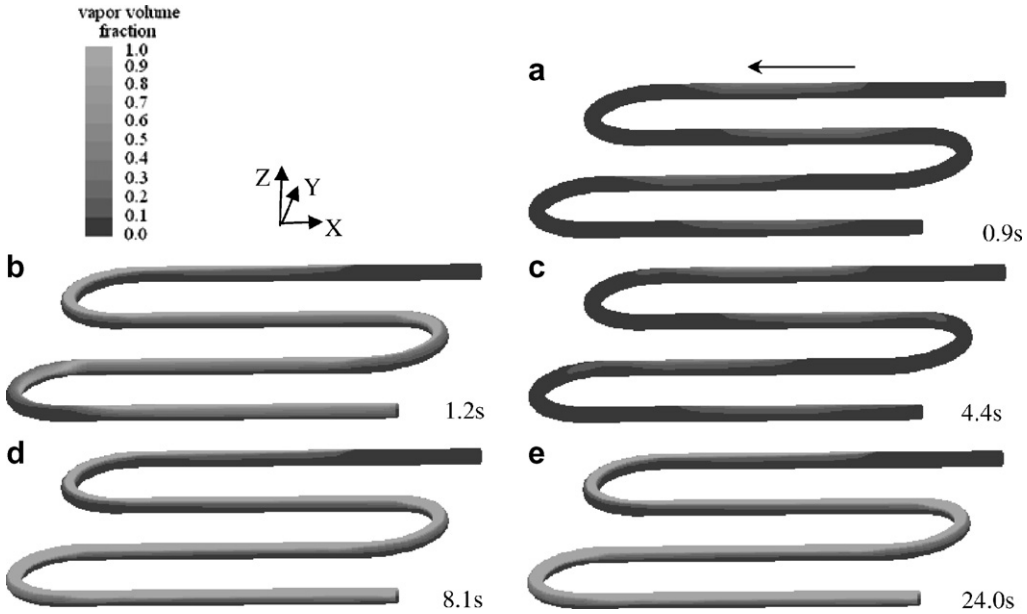

Fig. 8. Simulated near-wall vapor void fraction evolution for Case 3.

feature is established between the front and the rear parts of the bend. We expect that phase redistribution together with the consequent disturbance on the flow, may effectively mitigate the large circumferential wall temperature difference caused by stratified flow.

5. Discussion

5.1. Secondary flow and boiling nucleation

Fig. 9 shows the static pressure distribution and secondary flow development at the cross sections A–H for Case 3. All the cross sections are observed from upstream. The velocity magnitude is presented by the vector length. The pressure contours indicate roughly the two-phase interface. In the heat straight sections, the secondary flow shows there is a counter-flow vortex pair. This is induced by fluid temperature distributions, however, it has different orientation when the void fraction varies. When the void fraction is very low (section A–A or D–D), the secondary flow is very weak, but it shows liquid near the wall moving upwards, and liquid near the center line moving downwards. When the void fraction increases (section E–E or H–H), there is a relatively larger vapor space in the upper part of the tube, and the secondary flow is much stronger. There is also a vortex pair but having an opposite orientation, with liquid moving upward near the center line, and moving downward near the wall. The difference may be caused by the increased vapor entrainment effect near the center line when void fraction is higher.

At the middle of the bend (section B–B or F–F), the secondary flow presents "Dean-type" flow which is commonly observed in single-phase flow in curved pipes. It is induced by a counter-flow vortex pair, with the fluid transportation from inner bend to outer bend [23,24] near the centerline. This is mainly caused by centrifugal force. Obviously, its orientation has 90° change from the vortex pair in the straight sections. Though this is similar to "Dean-type" flow, it is somewhat different due to the influence of two-phase distribution and buoyancy. The two-phase interface at the U-bend tilts toward the inner bend, however, it recovers to be more horizontal after the bends. That means that though buoyant force is dominant in the system, the centrifugal force plays an important role at the U-bends.

From the experimental observations, the flow boiling process in a horizontal straight tube included boiling nucleation, upper part boiling, full nucleate boiling on the whole tube wall, upper film evaporation and lower part full nucleate boiling, uniformly tempestuous nucleate boiling, as the applied heat flux increased. These modes are expected to be closely dependent on the buoyancy force and pressure distribution. Our experimental observations indicate that the nucleation would easily happen at the top surface near the centerline. As shown in Fig. 9, static pressure gradient exists in the Z-axis direction due to density difference and gravity. This results in a slightly lower saturate temperature at the upper part of the tube, which may contribute to the easier nucleation occurrence there. Additionally, we anticipate some random disturbances or some non-condensable gas or remained vapor existing near the top centerline zone and serving as nucleation sites or catalysts.

5.2. Bend effect

The two-phase flow in the U-bends shows complicated phenomena, with various phase transition patterns (i.e., breakup and/or oscillation) and phase redistribution. Buoyancy is observed to play an important role in such horizontal bends. In addition, centrifugal force and inertia force also influence the phase distribution or transition. As the mass flux increases, or the void fraction decreases, the latter two factors have a significant effect to induce a twisted passage of the vapor phase. This will be shown in Section 5.3.

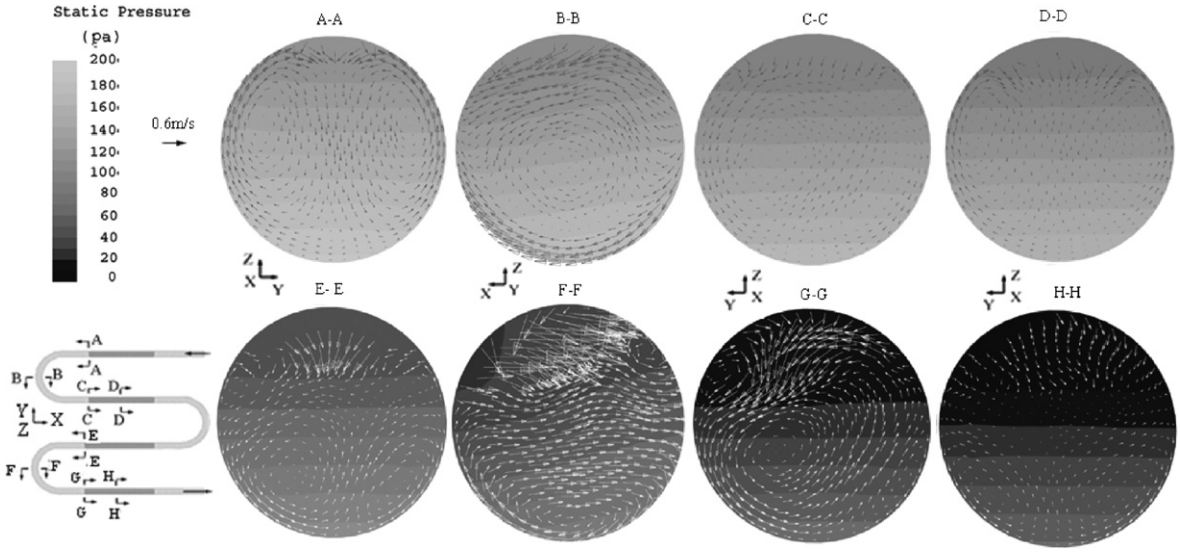

Fig. 9. Contours of static pressure and secondary flow velocity vector map at the cross sections A–E for Case 3.

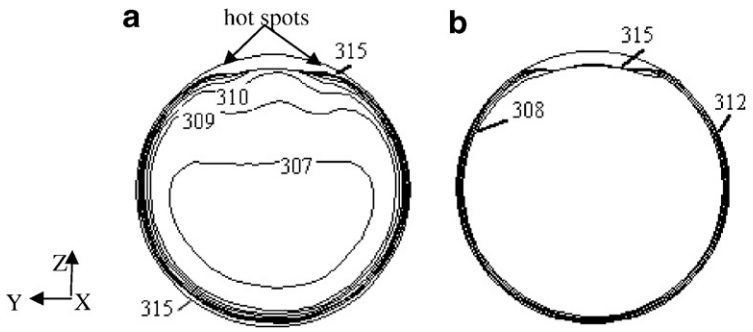

Fig. 10. Contours of fluid temperature at the cross sections of the second bend (unit: K): (a) bend entrance(cross section E–E in Fig. 9) and (b) bend exit.

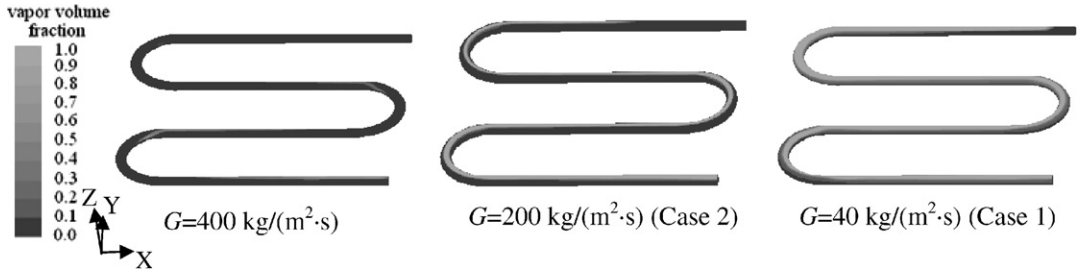

Fig. 11. Contours of near-wall void fraction at different mass fluxes.

The adiabatic U-bends may also have another function: amending the thermal non-equilibrium existing between the superheated vapor and the subcooled/saturated/superheated liquid in the flow boiling system. When the flow passes the heated straight tube sections, the liquid or vapor was partially or locally superheated. As the flow enters into the adiabatic bends, the mixing of the liquid with vapor results in re-condensation of vapor and heating of subcooled liquid. This creates a release of thermal non-equilibrium for the two-phase flow. As an experimental demonstration, some bubbles and slugs were observed shrunken and even collapsed as the two-phase flow passed through the bends. The simulation reveals this effect also. Fig. 10 shows the contours of liquid–vapor mixture temperature at the entrance and exit cross sections of the Second bend for Case 2. Temperature differences tended to decrease at the bend exit, implying the release of thermal non-equilibrium in the bend. The highest temperature exists at the two spots beside the top centerline of the tube, which is induced by the secondary flow.

5.3. Influence of mass flux

The mass flux is one of the most important factors determining the quality of the saturated mixture at exit. Fig. 11 compares the contours of the near-wall void fraction with different mass fluxes but with the same heat flux. As the mass flux increases, the vapor void fraction at exit decreases. Generally, at low mass flux or at the beginning of the boiling process, small vapor fraction is very likely to exist in the form of bubbles entrained by the continuum liquid flow. With the mass flux decreasing, the phase distribution is gradually dominated by the buoyant force, resulting in the stratification of the liquid and vapor phases. It may be predicted that in the transition with medium vapor fractions, the stratification is not stable, and the intermittent disturbance would disrupt the continuum of the vapor space and cause slug flow. As shown in Fig. 11, at a very low mass flux, the vapor phase generated in the first straight section is not only entrained downstream, but also expands upstream to the inlet, as observed in the experiments. Comparison of three cases shows that the twisted vapor passage in the U-bends is more apt to happen for small amount of vapor fractions.

6. Conclusions

Numerical simulation and experimental study were conducted to investigate the refrigerant flow boiling in a horizontal serpentine tube. The comparison indicates that both the experimental observation and numerical simulation are consistent with each other. Particularly, the simulation well explains the effects of phase redistribution and thermal non-equilibrium release observed in the experiments.

The liquid and vapor phase distributions show stratification in the horizontal tube, indicating the buoyancy force caused by the gravitational acceleration is dominant, especially when the vapor void fraction is sufficiently high. However, for low vapor void fractions, if the bubble nucleation and flow instability are considered, the vapor phase may be dispersed resulting in bubbly flow. The flow for small vapor fraction is very likely to exist in the form of bubbles entrained by the flow with the liquid as the continuum phase. With the mass flux decreasing and/or vapor

void fraction increasing, the phase distribution is gradually governed by the buoyant force, resulting in the stratification of the liquid and vapor phases. It may be expected that in the transition region with intermediate vapor fractions, the stratification is not stable, and the intermittent disturbance would disrupt the continuum of the vapor space, resulting in slug flow.

The U-bend has important influences on the refrigerant phase redistribution in the tube. Though being adiabatic, the bend sections served to redistribute the vapor phase induced by the geometric changes (which causes the centrifugal force) and re-condensation of the vapor generated from the thermal non-equilibrium between the two phases. The vapor prefers to accumulate to the inner part of the tube bend, forming a twisted vapor passage near the upper-inner part of the tube bend. Such phenomenon is more apt to happen for small amount of vapor fractions. The phase distribution displays somewhat quasi-symmetric flow between the front and the rear parts of the tube bend.

Based on our observations of two-phase refrigerant flow boiling in horizontal serpentine tubes, we envision the opportunity to improve heat exchanger performance by redesign of circuitry. Such circuitry could lead to preferred phase distribution and improved latent heat transfer.

Acknowledgements

This work is currently supported by Advanced Heat Transfer LLC, USA (http://www.advancedheattransfer.com). A special thank you goes to Dr. Steve Wayne, the CEO of AHT, for his valuable input and encouragement.

References

[1] O. Baker, Simultaneous flow of oil and gas, Oil Gas J. 53 (1954) 185–190.
[2] Y. Taitel, A.E. Dukler, A model for predicating flow regime transitions in horizontal and near horizontal gas–liquid flow, Am. Inst. Chem. Engrs. (AIChE) J. 22 (1976) 43–55.
[3] J.G. Collier, J.R. Thome, Convective Boiling and Condensation, third ed., Oxford Science Publications, 1996.
[4] T.G. Theofanous, T.J. Hanratty, Appendix 1: report of study group on flow regimes in multifluid flow, Int. J. Multiphase Flow 29 (2003) 1061–1068.
[5] K. Hashizume, Flow pattern and void fraction of refrigerant two-phase flow in a horizontal pipe, Bull. Jpn. Soc. Mech. Eng. (JSME) 26 (1983) 1597–1602.
[6] D. Steiner, Heat transfer to boiling saturated liquids, in: VDI-warmeatlas (VDI Heat Atlas) Verein Deutscher Ingenieure (Ed.), VDI-Gessellschaft Verfahrenstchnik und Chemieingenieurwesen (GCV), Dusseldorf, Germany, 1993 (J.W. Fullarton, Translator).
[7] N. Kattan, Contribution to the heat transfer analysis of substitute refrigerants in evaporator tubes with smooth and enhanced surfaces. Thesis No. 1498, Swiss Federal Institute of Technology, Lausanne, 1996.
[8] N. Kattan, J.R. Thome, D. Favrat, Flow boiling in horizontal tubes: part 1 – development of a diabatic two-phase flow pattern map, J. Heat Transfer 120 (1998) 140–147.
[9] N. Kattan, J.R. Thome, D. Favrat, Flow boiling in horizontal tubes: part 3 – development of a new heat transfer model based on flow pattern, J. Heat Transfer 120 (1998) 156–165.
[10] J.R. Thome, J.E. Hajal, Two-phase flow pattern map for evaporation in horizontal tubes: latest version, in: First International Conference on Heat Transfer, Fluid Mechanics and Thermodynamics, South Africa, 2002.
[11] L. Wojtan, Experimental and analytical investigation of void fraction and heat transfer during evaporation in horizontal tubes. Thesis No. 2978, Swiss Federal Institute of Technology, Lausanne, 2004.
[12] S.S. Kandlikar, A General Correlation For Saturated Two-Phase Flow Boiling Heat Transfer Inside Horizontal And Vertical Tubes. ASME Winter Annual Meeting, 1987.
[13] J.E. Hajal, J.R. Thome, A. Cavallini, Condensation in horizontal tubes, part 1: two-phase flow pattern map, Int. J. Heat Mass Transfer 46 (2003) 3349–3363.
[14] J.R. Thome, J.E. Hajal, A. Cavallini, Condensation in horizontal tubes, part 2: new heat transfer model based on flow regimes, Int. J. Heat Mass Transfer 46 (2003) 3365–3387.
[15] T.H. Shih, W.W. Liou, A. Shabbir, Z. Yang, J. Zhu, A new κ–ϵ eddy-viscosity model for high Reynolds number turbulent flows – model development and validation, Comput. Fluids 24 (1995) 227–238.
[16] Fluent Inc., Fluent 6 User Guide Manual, Lebanon, 2004.
[17] L. Schiller, Z. Naumann, Z. Ver. Deutsch. Ing. 77 (1935) 318.
[18] W.E. Ranz, W.R. Marshall Jr., Evaporation from drops, part I, Chem. Eng. Prog. 48 (1952) 141–146.
[19] W.E. Ranz, W.R. Marshall Jr., Evaporation from drops, part II, Chem. Eng. Prog. 48 (1952) 173–180.
[20] W.H. Lee, A pressure iteration scheme for two-phase flow modeling, in: T.N. Veziroglu (Ed.), Multiphase Transport Fundamentals, Reactor Safety, Applications, vol. 1, Hemisphere Publishing, Washingdon, DC, 1980.
[21] S.A. Vasquez, V.A. Ivanov, A phase coupled method for solving multiphase problems on unstructured meshes. in: Proceedings of ASME FEDSM'00: ASME 2000 Fluids Engineering Division Summer Meeting, Boston, 2000.
[22] Z. Rouhani, E. Axelsson, Calculation of void volume fraction in the subcooled and quality boiling regions, Int. J. Heat Mass Transfer 13 (1970) 383–393.
[23] W.R. Dean, Note on the motion of fluid in a curved pipe, Philos. Mag. 20 (1927) 208–223.
[24] H. Ito, Flow in curved pipes, JSME Int. J. 30 (1987) 543–551.